E-proceedings of the 36th IAHR World Congress
28 June – 3 July, 2015, The Hague, the Netherlands

TURBULENT ADVANCES OF BREAKING BORES: PHYSICAL MODELLING IN A LARGE FACILITY

XINQIAN LENG[(1)], & HUBERT CHANSON[(2)]

[(1)] *The University of Queensland, School of Civil Engineering, Brisbane QLD 4072, Australia*
e-mail: xinqian.leng@uqconnect.edu.au

[(2)] *The University of Queensland, School of Civil Engineering, Brisbane QLD 4072, Australia*
e-mail: h.chanson@uq.edu.au

ABSTRACT

In an estuarine system, the flood tidal wave may become a tidal bore during the early flood tide in a narrow funnelled channel under large tidal ranges. Herein new experiments were conducted in a large flume to investigate breaking tidal bores and the bore roller propagation. The results demonstrated several key features of tidal bores propagating in rectangular channels. The propagation of the breaking bore roller was a highly turbulent process. The celerity of the roller toe fluctuated rapidly with both longitudinal and transverse distances. The instantaneous longitudinal free-surface profile of the roller showed significant temporal and spatial fluctuations. The free-surface fluctuations were maximum shortly after the toe passage. The unsteady velocity measurements indicated large and rapid fluctuations of all velocity components during the bore passage. The velocity fluctuations yielded very significant Reynolds stress amplitudes and fluctuations. Instantaneous stress magnitudes in excess of 90 Pa were observed in laboratory, having the potential to scour large non-cohesive materials.

Keywords: *Breaking bores, Turbulence, Tidal bores, Physical modelling, Reynolds stresses*

1. INTRODUCTION

In an open channel, canal, river or estuary, a sudden increase in flow depth induces a positive surge, compression wave or bore (Henderson 1966, Bryson 1969, Liggett 1994). In an estuarine system, the flood tidal wave may become a tidal bore during the early flood tide in a narrow funnelled channel under large tidal ranges (Tricker 1965, Chanson 2011) (Fig. 1). After its onset, the bore may be analysed as a hydraulic jump in translation (Rayleigh 1908, Lighthill 1978). The shape of the surge is a function of its Froude number Fr_1 (Montes 1998, Chanson 2012):

$$Fr_1 = \frac{V_1 + \overline{U}}{\sqrt{g \frac{A_1}{B_1}}} \quad [1]$$

where V_1 is the initial flow velocity positive downstream, $\overline{U}$ is the bore celerity positive upstream, g is the gravity acceleration, A_1 is the initial flow cross-section area and B_1 is the initial free-surface width (Fig. 2). An undular surge is observed for $Fr_1 < 1.3$ to 1.5 (Fig. 1A). For $Fr_1 > 1.4$ to 1.6, the leading edge of the bore is characterised by a breaking roller (Fig. 1B). The bore roller is characterised by a sudden increase in water depth, a highly turbulent flow with large-scale vortical structures, some kinetic energy dissipation, a two-phase air-water flow region and strong turbulence interactions with the free surface associated with splashes and droplet ejections. For a stationary hydraulic jump, $\overline{U} = 0$ and the inflow Froude number becomes: $Fr_1 = V_1/(g\ A_1/B_1)^{1/2}$ (Chanson 2012).

Herein a physical investigation was conducted in laboratory with a focus on the bore roller properties. New experiments were conducted in a large size facility. The observations included a series of video observations of propagating breaking bores to characterise the roller toe perimeter, the bore front celerity and their fluctuations, some instantaneous velocity measurements during the roller passage, as well as some preliminary unsteady air entrainment measurements in the bore roller using a dual-tip phase-detection probe.

Figure 1. Tidal bores, with bore propagation from left to right (by Hubert Chanson). (A, Left) Undular tidal bore of the Dordogne River (France) on 20 October 2013; (B, Right) Breaking tidal bore of the Qiantang River (China) on 11 October 2014

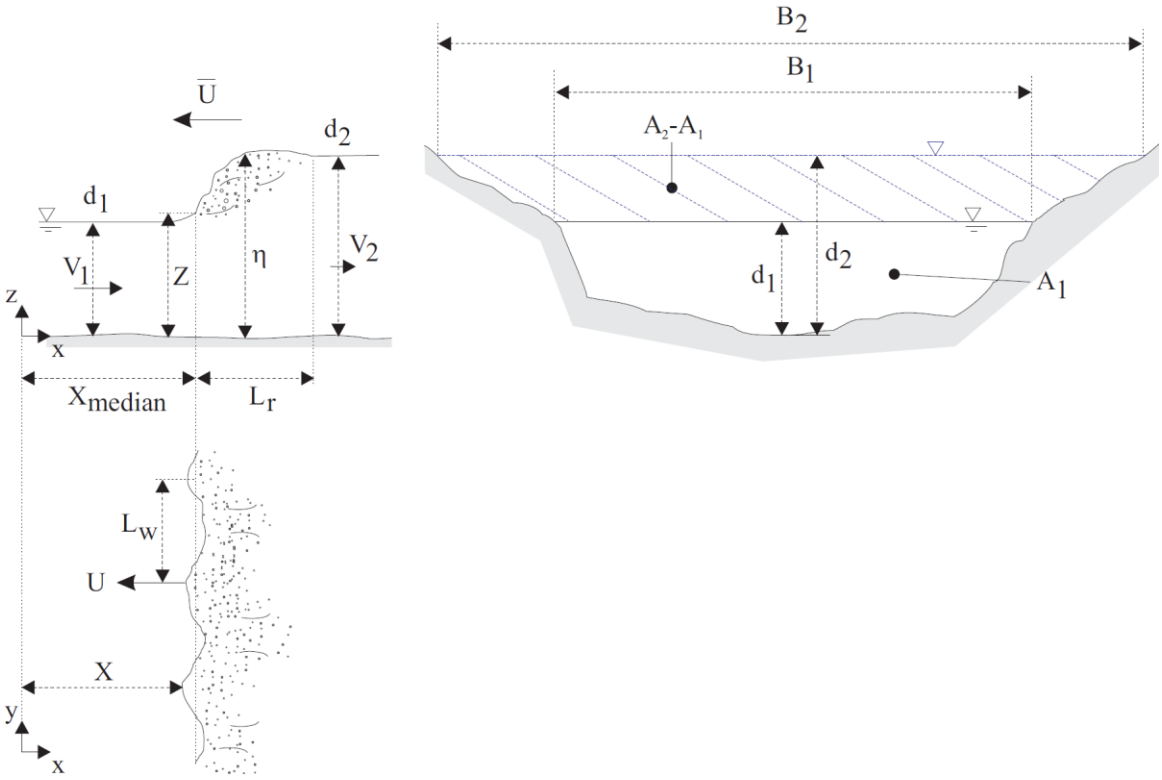

Figure 2. Definition sketch of a breaking tidal bore propagating in an irregular cross-section channel

2. PHYSICAL MODELLING, EXPERIMENTAL FACILITY AND INSTRUMENTATION

2.1 Dimensional considerations

Laboratory investigations may provide some detailed information on the physical processes, and some recent progresses in instrumentation offer means for successful unsteady turbulence measurements (Hornung et al. 1995, Koch and Chanson 2009). For a tidal bore propagating in a horizontal rectangular channel, a simplified dimensional analysis yields

a series of relationships between the dimensionless free-surface properties, and turbulent flow properties, at a given location (x, y, z) at time t as functions of a number of relevant dimensionless numbers characterising the fluid properties and physical constants, the channel geometry, and the initial and boundary conditions:

$$\frac{\eta}{d_1}, \frac{d_2}{d_1}, \frac{Z}{d_1}, \frac{L_w}{d_1}, \frac{L_r}{d_1} \ldots = f_1\left(\frac{x}{d_1}, \frac{y}{d_1}, t\sqrt{\frac{g}{d_1}}, \frac{V_1+\overline{U}}{\sqrt{g\,d_1}}, \rho\frac{(V_1+\overline{U})d_1}{\mu}, \frac{B}{d_1}, \frac{g\mu^4}{\rho\sigma^3}, \ldots\right) \quad [2]$$

$$\frac{P}{\rho g\, d_1}, \frac{V_x}{V_1}, \frac{V_y}{V_1}, \frac{V_z}{V_1}, \frac{v_x'}{V_1}, \frac{v_y'}{V_1}, \frac{v_z'}{V_1} \ldots = f_2\left(\frac{x}{d_1}, \frac{y}{d_1}, \frac{z}{d_1}, t\sqrt{\frac{g}{d_1}}, \frac{V_1+\overline{U}}{\sqrt{g\,d_1}}, \frac{v_1'}{V_1}, \rho\frac{(V_1+\overline{U})d_1}{\mu}, \frac{B}{d_1}, \frac{g\mu^4}{\rho\sigma^3}, \ldots\right) \quad [3]$$

where η is the free-surface elevation, d_2 is the conjugate depth, Z is the roller toe elevation, L_w is the transverse wave length, L_r is the roller length, d_1 is the initial depth, V_1 is the cross-sectional averaged initial velocity positive downstream, B is the channel width, g is the gravity acceleration, ρ and μ are the water density and dynamic viscosity respectively, and σ is the surface tension between air and water, P is pressure, V and v' are respectively the instantaneous mean velocity component, root mean square of velocity fluctuation and integral time scale, the subscripts x, y and z refer to the longitudinal, transverse and vertical velocity components, v_1' is the root mean square of velocity fluctuation in the initially steady flow. In Equation [2] ([3]) right handside, the 4th (5th) and 5th (7th) terms are the tidal bore Froude and Reynolds numbers respectively, and the last term is the Morton number, a function only of fluid properties and gravity constant. Note that, in Equations [2] and [3], the left handside includes only an incomplete characterisation of the unsteady flow properties while the right handside does not account for the effects of surfactants, bio-chemicals, sediments and aquatic life which are relevant in a natural system.

A true dynamic similarity is achieved in a geometrically similar model if and only if each dimensionless term has the same value in prototype and laboratory. Scale effects might occur when one or more terms have different values between laboratory and field. In a tidal bore, the gravity effects are important and a Froude similitude is typically used (Tricker 1965, Liggett 1994). In the present study, both Froude and Morton similitudes were adopted following Hornung et al. (1995) and Koch and Chanson (2009). The laboratory investigation was performed in a relatively large-size facility to ensure that the results may be extrapolated to full-scale with negligible viscous scale effects.

2.2 Experimental facility and instrumentation

New experiments were conducted in a large tilting channel, made of glass sidewalls and smooth PVC bed. The channel ended with a free overfall. The initially steady flow was delivered into an upstream intake channel and led to the 19 m long 0.7 m wide glass sidewalled test section through a series of flow straighteners followed by a smooth bed and sidewall convergent. A fast-closing Tainter gate was located next to the test section's downstream end (x = 18.1 m), where x is the horizontal distance from the upstream end of the flume.

The video observations were conducted using a HD video camera Sony HDR-XR160, operating at 25 fps or 50 fps, with a resolution of 1920×1080 pixels, and a digital camera Casio Exlim EX-10, set at 120 fps (640×480 pixels), 240 fps (512×384 pixels) or 480 fps (224×160 pixels). The video camera was mounted vertically looking down across the channel width at about x = 6.6 to 6.7 m (Sony HDR-XR160) and x = 9.2 m (Casio Exlim EX-10). A two-bulb fluorescent light was used to achieve a fast shutter speed. Photographic sequences in high-speed continuously shooting mode (8.3 fps) were taken through the sidewalls to capture the instantaneous free-surface profiles during the bore front passage (Fig 2-1C). The dSLR camera was a Pentax K-3 (6016×4000 pixels) with Carl Zeiss Distagon 28 mm f2 lens, producing photographs with a low degree (< 1%) of barrel distortion. Both the video movies and dSLR photographs were analysed manually to guarantee maximum reliability of the data.

In steady flows, the water depths were measured using pointer gauges. The unsteady water depths were recorded with a series of acoustic displacement meters. A Microsonic Mic+35/IU/TC unit was located at x = 18.17 m immediately downstream of the Tainter gate. Further nine acoustic displacement meters Microsonic Mic+25/IU/TC were spaced along the channel at x = 17.81 m, 17.41 m, 14.96 m, 12.46 m, 9.96 m, 8.5 m, 6.96 m, 3.96 m and 0.96 m. All acoustic displacement meters (ADMs) were calibrated against the pointer gauge in steady flows.In steady and unsteady flows, the velocity measurements were conducted with an acoustic Doppler velocimeter (ADV) Nortek™ Vectrino+ (Serial No. VNO 0436) equipped with a three-dimensional sidelooking head at a range of vertical elevations z throughout the water column. The ADV was located at x = 8.5 m on the channel centreline. The velocity range was ±1.0 m/s and the data accuracy was 1% of the velocity range. The ADV was set up with a transmit length of 0.3 mm and a sampling volume of 1.5 mm height. Both the acoustic displacement meters and acoustic Doppler velocimeter were synchronised within ± 1 ms, and they were sampled simultaneously at 200 Hz using a high-speed data acquisition system USB NI 6212 BNC. In steady flows, the ADV post processing included the removal of communication errors, the removal of average signal to noise ratio data less than 5 dB and the removal of average correlation values less than 60%. In addition, the phase-space thresholding technique developed by Goring and Nikora (2002) and implemented by Wahl (2003) was used to remove spurious points in the data set. In unsteady flow conditions, the above post-processing technique was not applicable (Chanson 2010, Koch and Chanson 2009). The unsteady flow post-processing was limited to a removal of

communication errors, and it is acknowledged that the vertical velocity component V_z data might be affected adversely by the bed proximity for $z < 0.030$ m.

During the air entrainment experiments, a dual-tip phase-detection conductivity probe was used to detect the air bubbles in the breaking roller. The sensor size was 0.25 mm and the longitudinal distance between the two tips was 6.5 mm. The dual-tip probe was excited by an electronic system (Ref. UQ82.518) designed with a response time of less than 10 μs. The vertical elevation of the probe was controlled by a Mitutoyo digimatic scale unit with an accuracy of 0.01 mm. The probe sampling rate was 40 kHz per sensor and the probe signal output was processed manually. The conductivity probe was placed at x = 7.1 m facing downstream and the measurements were performed at several elevations, typically above the initial water level. The data at different vertical elevations were synchronised using sideview photographs taken simultaneously, yielding the median free-surface elevations as a function of x-X, where X is the instantaneous roller toe longitudinal location. Further details on the experimental facility and instrumentation were reported in Leng and Chanson (2014).

2.3 Experimental procedure

For all experiments, the breaking bores were generated by the fast closure of the Tainter gate and the bore propagated upstream against the initially-steady flow. Figure 3 illustrates some photograph of advancing breaking bore. Chanson and Toi (2015) presented a thorough model-prototype comparison, highlighting a sound agreement in terms of dimensionless instantaneous free-surface and velocity data between laboratory and field observations.

Figure 3. Laboratory experiment: side views of the advancing bore roller with a time interval of 0.12 s between photographs ($Fr_1 = 1.38$, $d_1 = 0.160$ m) (shutter speed: 1/4,000 s) - Bore propagation from left to right - Note the phase-detection probe on the top right

3. EXPERIMENTAL OBSERVATIONS: BORE ROLLER CHARACTERISTICS

3.1 Presentation

In breaking tidal bores, the roller toe is a flow singularity where vorticity is generated and air is entrapped (Hornung et al. 1995, Brocchini and Peregrine 2001). Figure 3 shows high-shutter speed side views of a roller toe. View in elevation, the roller toe formed a continuous line, herein called the roller toe perimeter (Fig. 2 & 4). The shape of roller toe perimeter was investigated in details including its evolution with time. For a series of experiments, video movies were digitalised frame-by-frame to extract the instantaneous toe perimeter. The data showed a broad range of instantaneous shapes (Fig. 4). Figure 4 presents typical transverse profiles of the toe perimeter, where x = X is the instantaneous toe location at a transverse distance y with y = 0 at the left side wall. On average the roller toe was quasi two-dimensional, but its shape evolved very rapidly with both transverse direction and time. The data demonstrated in particular some backshifts of roller toe location, indicating that the toe occasionally shifted backwards for a very short period of time with a negative instantaneous celerity (e.g. Fig. 4, t ~ 0.06 s). The deviations of the roller toe perimeter about the instantaneous cross-sectional median position X_{median} were calculated, and the results indicated some quasi-periodic fluctuation of the toe perimeter in the transverse direction. The data exhibited a quasi-normal distribution and the results were basically independent of the movie frame rate, yielding $(X-X_{median})'/d_1 = 0.145$ on average at a given time, where $(X-X_{median})'$ is the standard deviation of the deviations of roller toe perimeter about the instantaneous cross-sectional median.

The transverse profile of the roller toe perimeter showed some pseudo-periodic shape (Fig. 4), indicating the existence of non-linear structures, streamwise vortices and streaks. The present observations suggested a phenomenon very similar to that observed in plane mixing layers and wall jets (Bernal and Roshko 1986). At a fixed time, the fluctuations of toe perimeter location around its median were analysed in terms of relevant transverse wave lengths L_w, see definition in Figure 2. The results indicated a predominant wave length about $L_w/d_1 = 1.2$. For comparison, the breaking bore of the Qiantang River (China) was observed in September 2013 (Leng and Chanson 2014). The data analysis yielded a dimensionless standard deviation $(X-X_{median})'/d_1$ was about 0.13, and the present laboratory observations compared well with the field observations. The transverse variations of instantaneous toe perimeter presented some pseudo-periodic fluctuations in the Qiantang River within the range $0.7 < L_w/d_1 < 25$; two dominant dimensionless wave lengths were L_w/d_1 ~ 1 and 5-10.

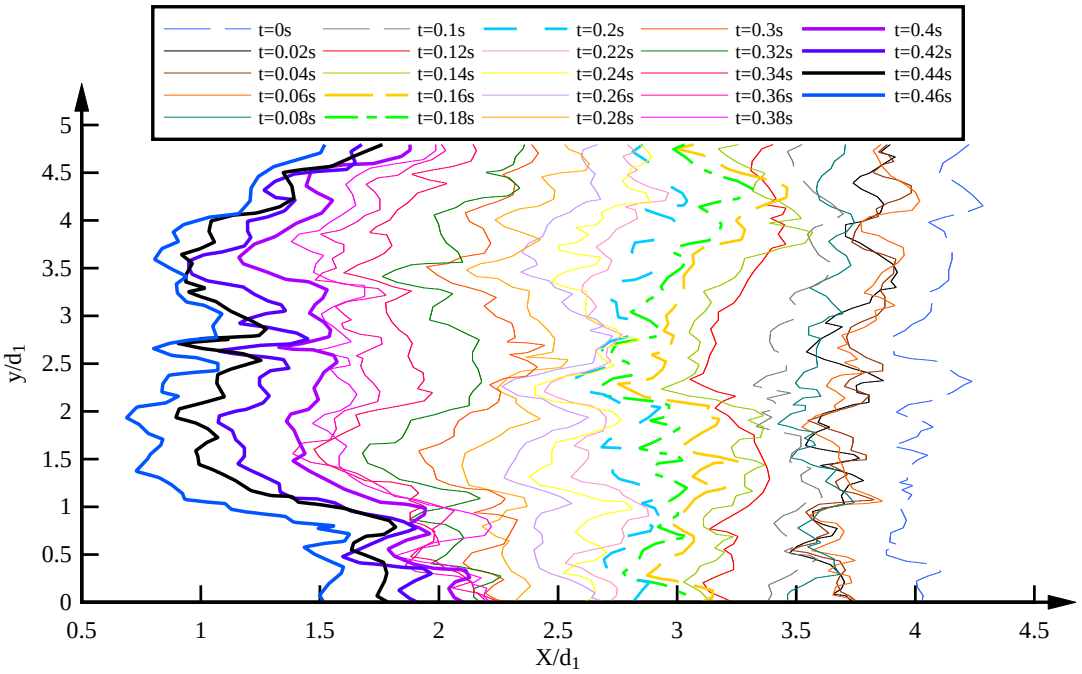

Figure 4. Instantaneous roller toe perimeter as function of time (Fr_1 = 1.49, d_1 = 0.146 m) - Bore propagation from left to right

3.2 Longitudinal roller profile

The instantaneous longitudinal roller surface profiles were documented using high-shutter speed photographs, as seen in Figure 3. The data highlighted the rapid fluctuations in roller surface elevations and the rapid changes in longitudinal roller profiles with time. The instantaneous free-surface fluctuations were herein described in terms of the differences between third and first quartiles (d_{75}-d_{25}). For a Gaussian distribution of the data set about its mean, (d_{75}-d_{25}) would be equal respectively to 1.3 times the standard deviation (Spiegel 1972). The present data indicated a maximum in free-surface fluctuations in the first half of the roller, as previously reported in hydraulic jumps with a breaking roller. The present results $(d_{75}\text{-}d_{25})_{max}$ are reported in Figure 5 and compared with previous studies of maximum turbulent fluctuations η'_{max} of the free-surface in stationary hydraulic jumps and in breaking tidal bores. The experimental data highlighted increasing free-surface fluctuations with increasing Froude number, and the results were comparable between breaking bores and stationary hydraulic jumps for some similar Froude number (Fig. 5).

The visual observations showed that the free-surface elevation first rose slowly immediately prior to the roller, for Froude numbers less than 2, as seen in Figure 3. Such an upward streamline curvature may be derived from theoretical considerations, namely the integral balances of linear momentum, in both horizontal and vertical directions, and of angular momentum (Valiani 1987). Such a gradual rise in free-surface ahead of the turbulent roller was previously observed (Hornung et al. 1995, Koch and Chanson 2009, Docherty and Chanson 2012). The vertical elevation Z of the roller toe was recorded and the data were compared with re-analysed breaking tidal bore data. The results are presented in Figure 6. Figure 6 regroups the dimensionless median toe elevation Z_{median}/d_1 and toe elevation fluctuations $(Z_{75}\text{-}Z_{25})/d_1$ data as functions of the Froude number, where Z_{75} and Z_{25} are the third and first quartiles respectively. Despite some difference in measurement techniques and boundary flow conditions, the experimental data showed a decrease in roller toe elevation with increasing Froude number. The data were best correlated by:

$$\frac{Z_{median}}{d_1} - 1 = 0.1854 \exp(-3.52(Fr_1 - 1.3)) \quad [4]$$

with a normalised correlation coefficient of 0.823 and a standard error of 0.033 (Fig. 6). The fluctuations in vertical elevation of roller toe showed also a decreasing trend with increasing Froude number. The results are shown in Figure 6 in terms of the difference between third and first quartiles. The data were correlated by:

$$\frac{Z_{75} - Z_{25}}{d_1} = 0.105 \exp(-1.99(Fr_1 - 1.3)) \quad [5]$$

with a normalised correlation coefficient of 0.835 and a standard error of 0.0168. Both Equations (3-1) and (3-2) are compared with breaking bore data in Figure 6. The asymptotic limits of the data indicated two distinct trends. For $Fr_1 < 1.3$, the bore was undular and the roller disappeared. For $Fr_1 > 2$, the dimensionless roller toe elevation Z/d_1 tended to unity and the fluctuations in roller toe elevation tended to small values corresponding to the initial free-surface fluctuations.

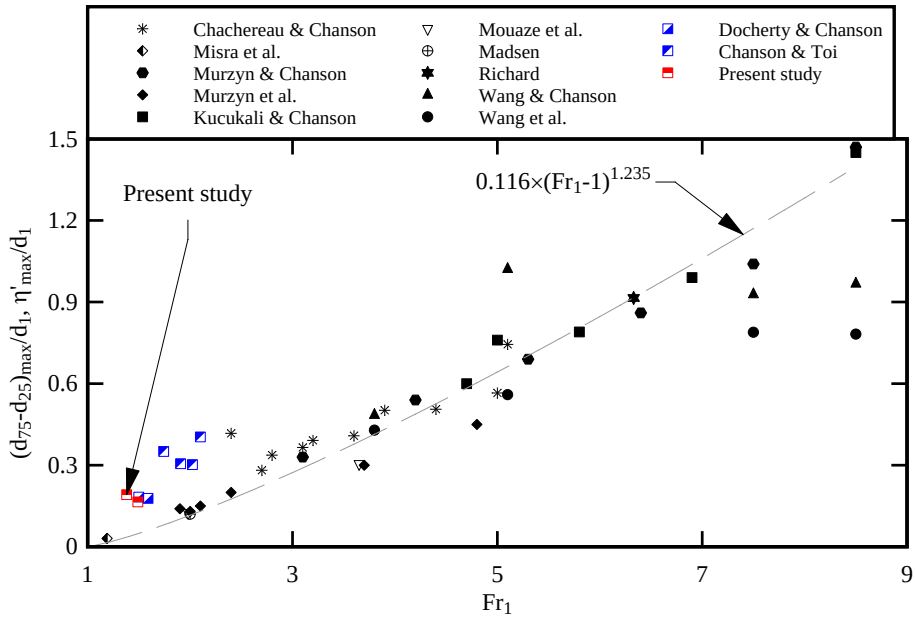

Figure 5. Maximum free-surface fluctuations in breaking tidal bores and hydraulic jumps - Tidal bore data: $(d_{75}\text{-}d_{25})_{max}/d_1$, Docherty and Chanson (2012), Chanson and Toi (2015), Present study (white, blue and red squares) - Hydraulic jump data η'_{max}/d_1: theoretical calculations (Richard 2013), experimental data (Madsen 1981, Mouaze et al. 2005, Misra et al. 2006, Murzyn et al. 2007, Kucukali and Chanson 2008, Murzyn and Chanson 2009, Chachereau and Chanson 2011, Wang and Chanson 2013, Wang et al. 2014)

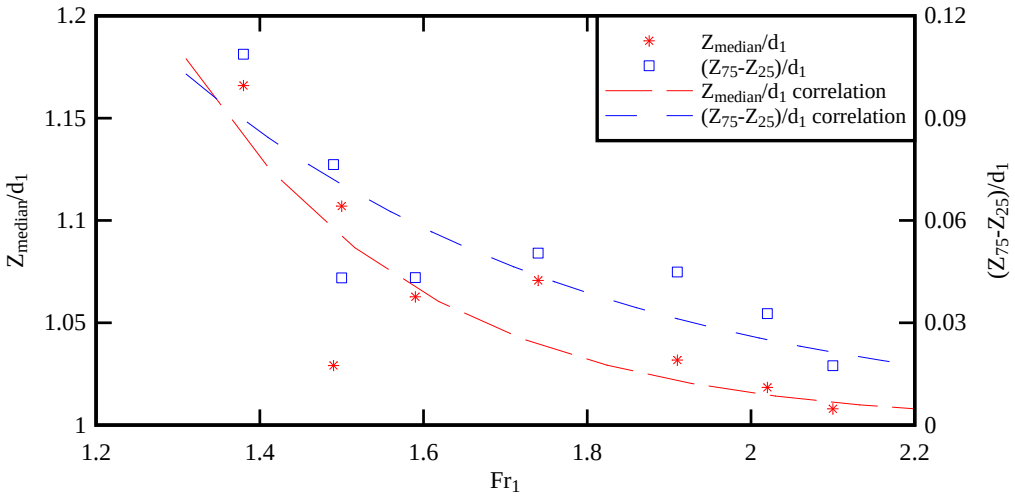

Figure 6. Fluctuations in vertical elevations Z/d_1 of the roller toe: median roller toe elevation and difference between third and first quartiles (Docherty and Chanson 2012, Chanson and Toi 2015, Present data) - Comparison with Equations [4] and [5] respectively

3.3 Bore roller celerity

The bore roller celerity was calculated based upon the instantaneous roller toe positions. The channel width was divided into seven 0.1 m wide sub-sections, and the mean celerity of each individual sub-section was estimated as a function of time. Typical statistical results are shown in Figure 7, including temporal mean, standard deviation, skewness and kurtosis, where B is the channel width (B = 0.7 m). The laboratory data indicated no sidewall effect. The results showed however large fluctuations in bore celerity with the ratio of standard deviation to temporal mean U'/U_{mean} between 0.6 and 1.6, with an average of all data about 1.0 (Fig. 7B)

The instantaneous cross-sectional averaged celerity $\overline{U}$ was derived from the median perimeter data of bore roller. For the data shown in Figure 7, the instantaneous cross-sectional averaged celerity fluctuated rapidly with time about a median value of approximately $\overline{U} \approx 0.95$ m/s. Yeh and Mok (1990) reported fluctuations in bore celerity during the propagation, although with lesser fluctuation magnitudes. The instantaneous celerity was not always positive, as seen for a few points in Figure 7A. These negative celerity data were consistent with some intermittent backshifts of the instantaneous roller toe perimeter discussed earlier. They might be related to the generation and advection of turbulent vortices in the roller as well as air bubble entrainment at the roller toe. The data showed typically similar outcomes for video frame rates of 50, 120, 240 and 480 fps, while The data at 25 fps tended to show some quantitative differences, likely caused by the sub-sampling.

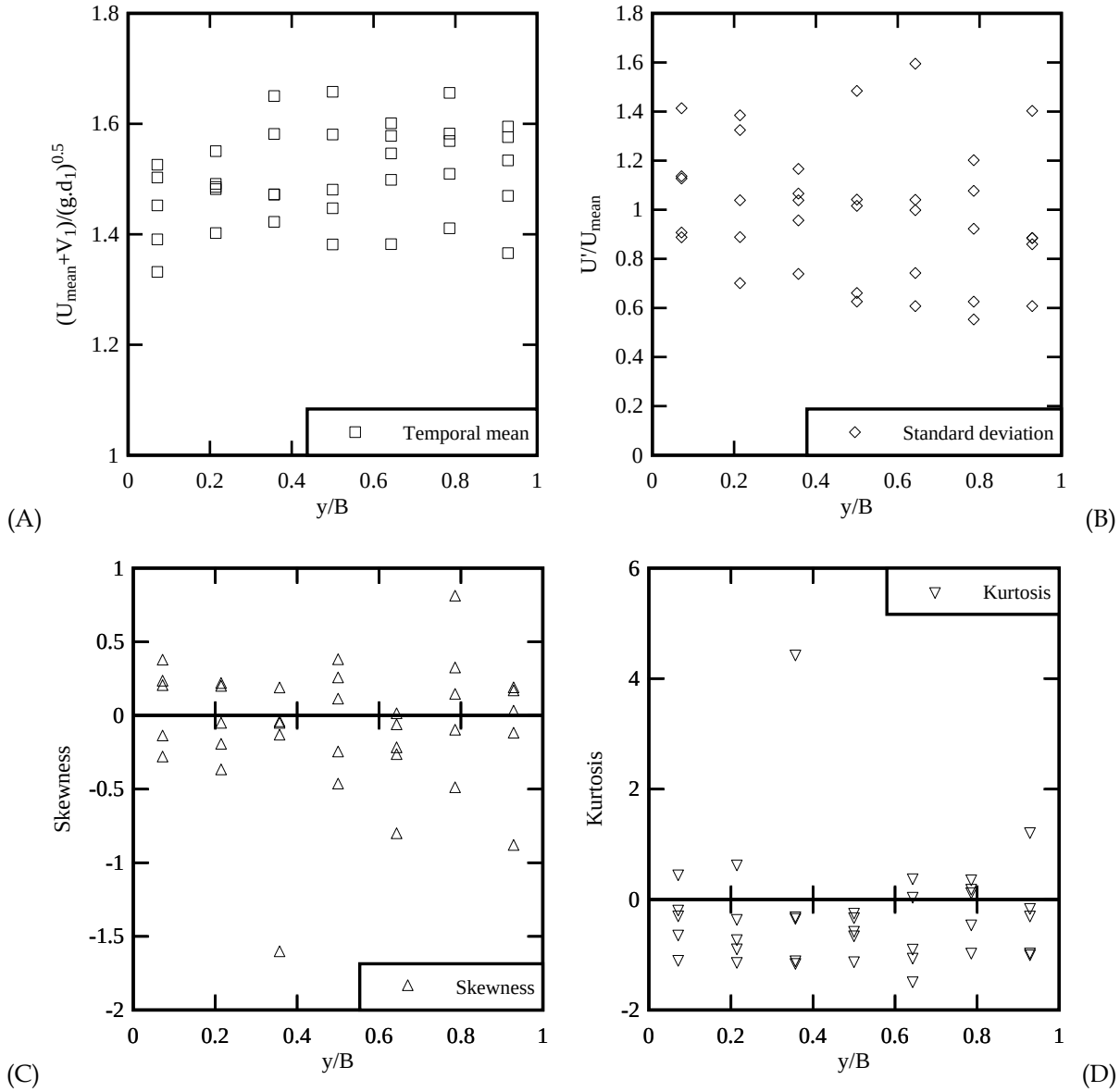

Figure 7. Transverse variations in roller toe celerity statistics (Fr_1 = 1.49, d_1 = 0.146 m, 50 fps movies) - each data point is an average over the video duration

4. UNSTEADY FREE-SURFACE AND VELOCITY MEASUREMENTS

4.1 Presentation

Ensemble-averaged unsteady free-surface and velocity measurements were conducted in the present study. Table 1 summarised the experimental flow conditions. Both breaking and undular bores were investigated. Breaking bores were observed when the bore Froude number $Fr_1 > 1.2$ to 1.3. For $Fr_1 > 1.4$ to 1.5, the secondary waves disappeared and the bore was characterised by a steep wall of water with a sharp breaking front. For $1 < Fr_1 < 1.1$ to 1.3, the bore was undular. Figure 8 shows typical side views of the propagation of a breaking bore (Fr_1 = 1.6) and undular bore with shock waves developing at the free-surface (Fr_1 = 1.2), respectively.

Visual, video and photographic observations highlighted the propagation process of a breaking bore was highly unsteady turbulent, with abrupt rise in free-surface elevations and rapidly fluctuating breaking rollers (Leng and Chanson 2014). The initially steady free-surface curved up slightly before the arrival of the roller toe for Froude numbers smaller than 2. For Froude numbers greater than 2, this upward streamline curvature was not seen. The breaking rollers were characterised by a two-phase air-water flow region and strong turbulent interactions, with free-surface splashes and droplet ejection. The free-surface was nearly horizontal behind the roller, although with some large fluctuations. The undular bores were characterised by a marked upward free-surface curvature ahead of the first wave crest, followed by a series of smooth undulations. For a Froude number between 1.2 and 1.3, undular bores with small shock waves developing at the free-surface were observed. The shock waves initiated from sidewalls upstream of the first wave crest, and intersected with the first wave crest on the centreline of the channel at the first wave crest.

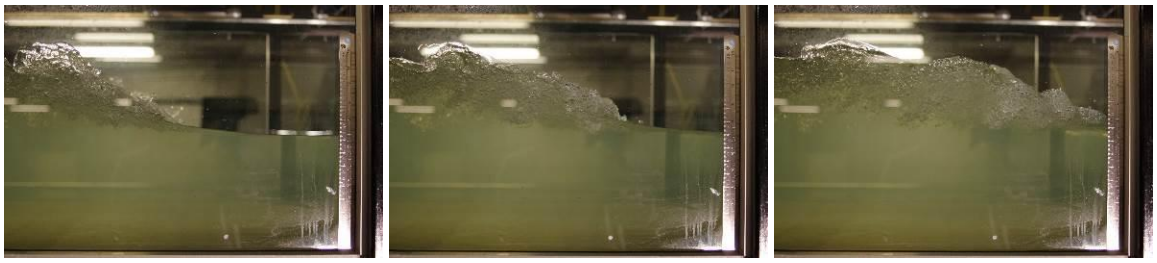

(A) Q=0.101 m^3/s, $S_o = 0$, Radial gate opening = 0 m, h= 0 m, $Fr_1 = 1.6$

(B) Q= 0.101 m^3/s, $S_o = 0$, Radial gate opening = 0.125 m, h = 0.071 m, $Fr_1 = 1.2$

Figure 8. Photographs of bore propagation from left to right, viewed from the side with a time interval of 0.12s between photographs

Table 1. Experimental flow conditions of ensemble-averaged free-surface and velocity measurements.

Q (m^3/s)	S_o	Radial gate opening (m)	h (m)	Surge type	d_1 (m)	Fr_1	Instrumentation
0.101	0	0	0	Breaking	0.175	1.5	Acoustic displacement meters & ADV velocimeter
		0.125	0.071	Undular	0.204	1.2	
	0.0075	0	0	Breaking	0.099	2.2	
0.055	0	0. 051	0.017	Undular	0.197	1.2	Acoustic displacement meters & ADV velocimeter
	0.005	0	0.051	Breaking	0.073	1.5	

4.2 Ensemble-averaged free-surface and velocity measurements

Ensemble-averaged free-surface measurements were conducted using a series of acoustic displacement meters (ADM) installed at different longitudinal locations along the flume centreline. The measurements were repeated 25 times for each flow condition, and the results were ensemble-averaged. Figure 9 presents some typical ensemble-averaged free-surface variations and fluctuations as functions of time for breaking and undular bores, respectively. The solid black line in each figure denotes the ensemble-averaged median free-surface elevation at x = 8.5 m. Overall, the ensemble-averaged free-surface measurements data highlighted the abrupt increase in water level associated with the passage of a breaking bore roller, and a significant upwards free-surface curvature with a train of secondary undulations following the passage of an undular bore. The free-surface fluctuations were quantified in terms of the difference between the third and first quartiles d_{75}-d_{25}. The propagation of a breaking bore was typically associated with higher maximum free-surface fluctuations, which was possibly caused by the highly turbulent breaking rollers (Fig. 9 left). For all experimental conditions, the results showed an increase in free-surface fluctuations following the propagation of a tidal bore. With breaking tidal bores, the free-surface fluctuations showed a marked maximum $(d_{75}\text{-}d_{25})_{max}$ shortly after the passage of the bore breaking roller (Fig. 9 left). With undular tidal bores, the first local maximum free-surface fluctuation occurred shortly after the passage of the first wave crest, followed by a series of local maximum fluctuations appearing in a quasi-periodic manner after the initiation of each secondary undulation (Fig. 9 right). The time-variations of the free-surface fluctuations in undular bores oscillated approximately in phase with the oscillations of the free-surface elevation.

A number of ensemble-averaged velocity measurements were conducted at x = 8.5 m using an acoustic Doppler velocimeter (ADV). Both breaking and undular bores were studied. The measurements were performed at three vertical elevations $z/d_1 = 0.1$, 0.4, and 0.8, where d_1 is the initial steady flow water depth. For each controlled flow condition, experiments were repeated 25 times and the results were ensemble-averaged. Figure 10 presents some typical ensemble-averaged velocity data for both breaking and undular bores, with the ensemble-averaged median water depth at the velocity sampling location as reference, highlighted by the black solid line. The turbulent velocity fluctuations were characterised by the difference between the third and first quartile V_{75}-V_{25} of the total ensemble. For a Gaussian distribution of an ensemble around its mean, V_{75}-V_{25} is equal to 1.3 of the standard deviation (Spiegel 1972). For both breaking and undular bores, the data showed a rapid deceleration of the longitudinal velocity component V_x at all vertical elevations. The data also indicated an abrupt acceleration and then deceleration of the vertical velocity component V_z, this effect being more important at higher vertical elevations. The results highlighted an increase in velocity fluctuations for all three velocity components at all elevations associated with the passage of both types of bores. At lower vertical elevations ($z/d_1 = 0.1$), higher velocity fluctuations were observed and the vertical velocity fluctuations were overall higher than the other two components for the same flow condition, most remarkably seen in the upper water column ($z/d_1 = 0.8$). In breaking bores, marked peaks in fluctuations of all three velocity components occurred slightly after the arrival of the bore front, whereas in undular bores, local maximum fluctuations appeared repetitively following the train of undulations. The results highlighted that the vertical velocity component was typically associated with the largest magnitude in

maximum fluctuations. For the same velocity component, breaking bores with higher Froude numbers tended to have higher values of maximum fluctuations than undular bores or breaking bore of lower Froude numbers. The time lag, defined as the time difference between the arrival of the breaking bore roller and the occurrence of the maximum velocity fluctuation, was larger in the upper water column comparing to that observed in mid and lower water columns.

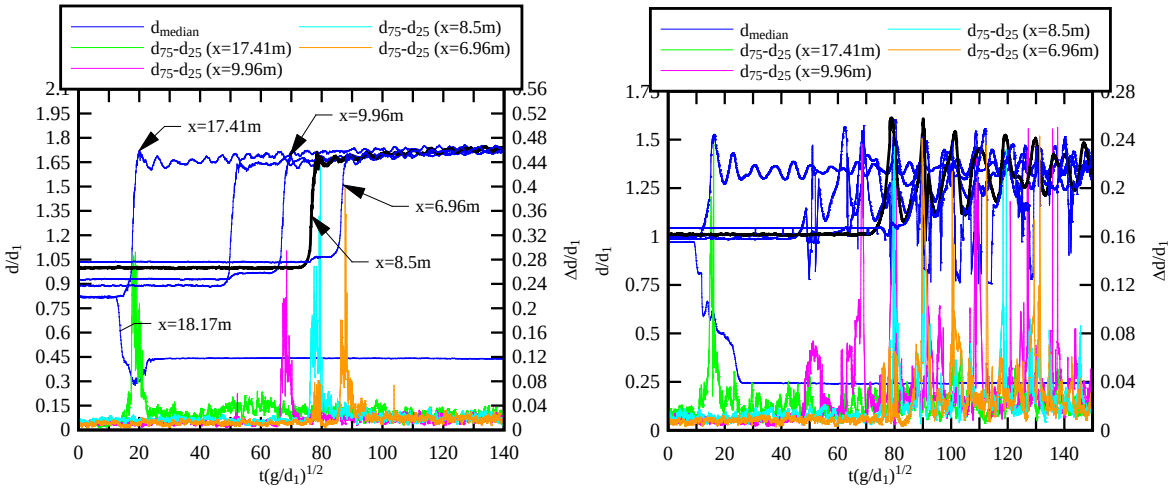

Figure 9. Ensemble-averaged time variations of median free-surface elevations and fluctuations at different longitudinal locations for breaking (left, Q = 0.101 m^3/s, Fr_1 = 1.5) and undular bores (right, Q = 0.101 m^3/s, Fr_1 = 1.2); Dimensionless time = 0 at gate closure.

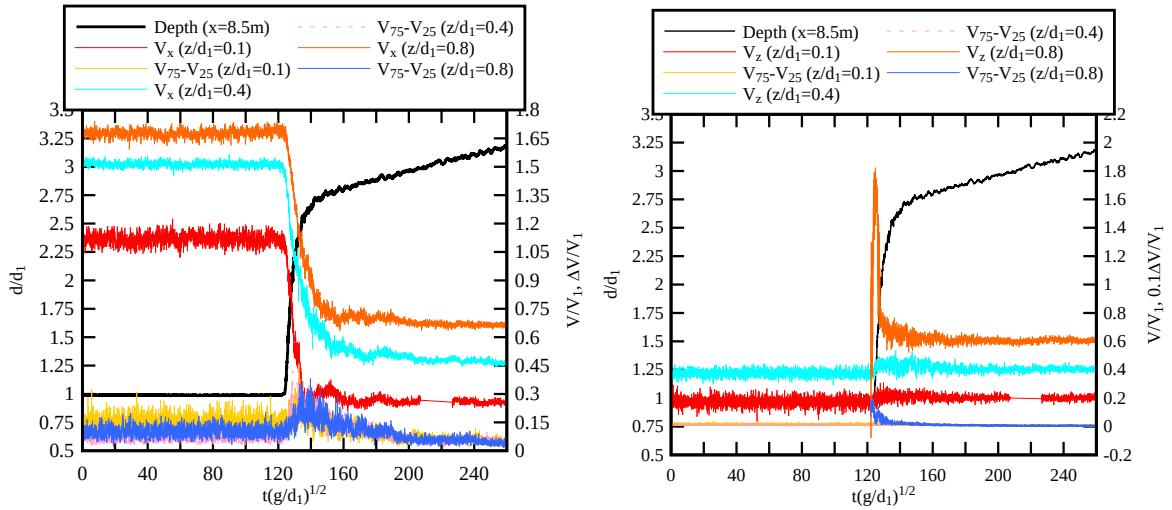

(A) Q = 0.101 m^3/s, Fr_1 = 2.2

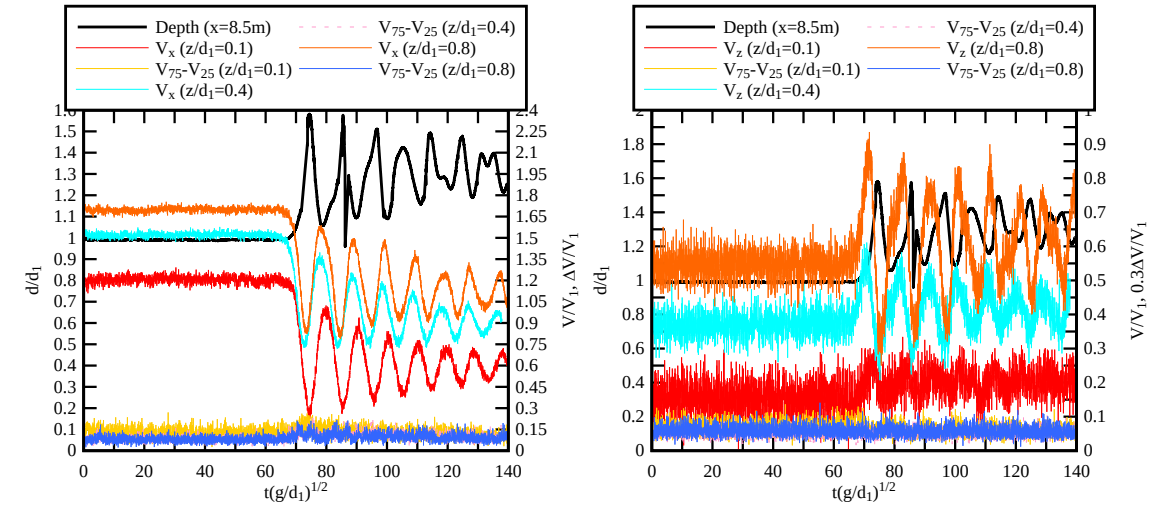

(B) Q = 0.101 m^3/s, Fr_1 = 2.2

Figure 10. Ensemble-averaged time variations of the median longitudinal velocity V_x and vertical velocity V_z with velocity fluctuations V_{75}-V_{25} at different vertical elevations z/d_1 for breaking (A) and undular (B) bores; Velocity data offset by +0.2 for all elevations; Dimensionless time = 0 at gate closure.

5. DISCUSSION

Herein, the Reynolds stress tensors were calculated based upon the deviation between the measured instantaneous velocity and the ensemble-average median. Figures 11 and 12 present typical time variations of the ensemble-averaged Reynolds stresses, the third quartile of the normal stresses (eg. $(v_xv_x)_{75}$) and the difference between the third and first quartiles of the tangential stresses (eg. $(v_xv_y)_{75}$-$(v_xv_y)_{25}$) for a breaking bores and undular bores, respectively. The solid black line denotes the ensemble-median free-surface variations. The third quartile of the normal stresses and the difference between the third and first quartiles of the tangential stresses characterised the fluctuations in shear stresses during the propagation of a tidal bore.

Overall, the results suggested that the propagation of a breaking bore was associated with significant increase in magnitudes and fluctuations in terms of both normal and tangential Reynolds stresses for all vertical elevations over the range of Froude numbers. Maximum stresses were highlighted in both normal and tangential stress tensors shortly after the passage of the bore breaking roller. The Reynolds stress data for an undular bore showed a similar trend to that of breaking bores, but with less pronounced peaks in the normal stress tensors. The stress magnitudes were smaller in undular bores comparing to breaking bores with the same discharge. Maximum instantaneous shear stresses were observed to occur shortly after the rise of the free-surface with magnitudes of up to 90 Pa for the range of experimental flow conditions. The results indicated the potential of sediment motion to occur beneath a tidal bore. For non-cohesive particles (Shields 1936, Yalin and Karahan 1979), large particles of up to 50 mm in size could be transported into motion under a maximum instantaneous shear stress of 90 Pa at laboratory scale.

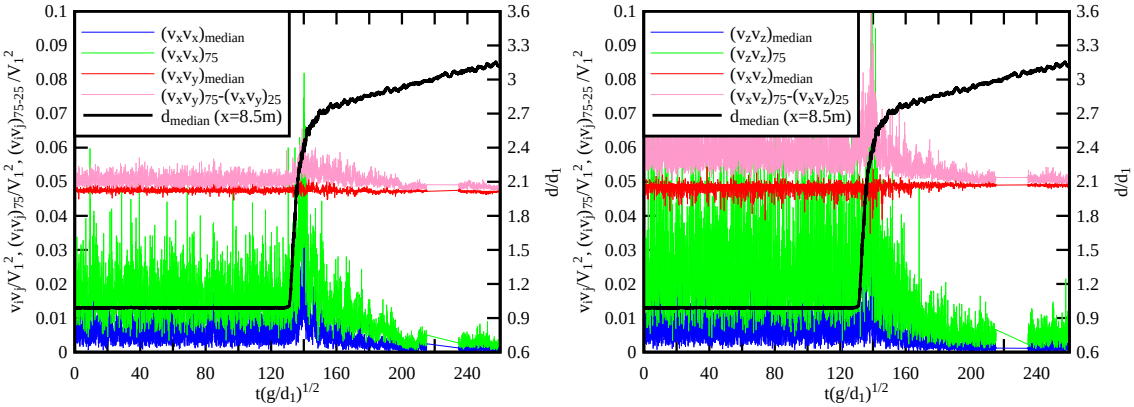

Figure 11. Time variations of the ensemble-averaged median Reynolds stresses, third quartile of the normal stresses and difference between the third and first quartiles of the tangential stresses for flow condition: Q = 0.101 m³/s, Fr_1 = 2.2, z/d_1 = 0.1; Tangential stresses and difference between the third and first quartiles of the tangential stresses were offset by +0.1m²/s²; Dimensionless time = 0 at gate closure.

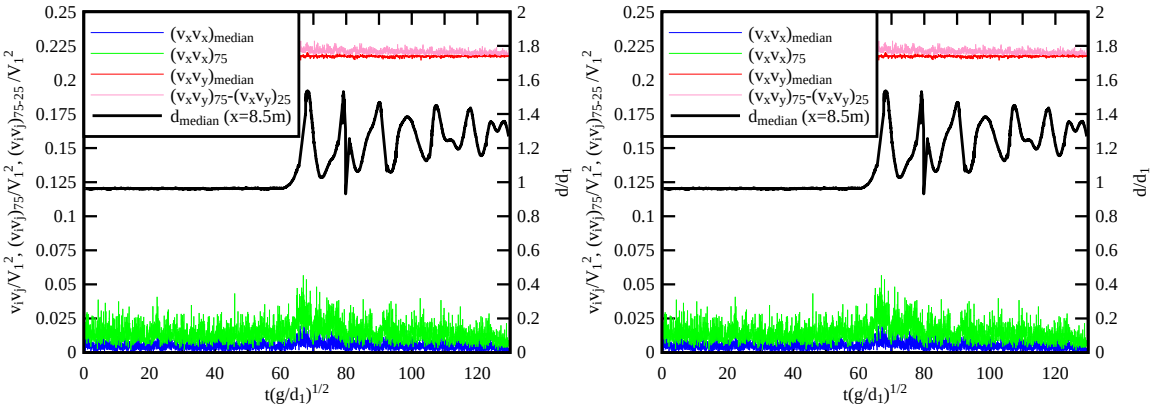

Figure 12. Time variations of the ensemble-averaged median Reynolds stresses, third quartile of the normal stresses and difference between the third and first quartiles of the tangential stresses for flow condition: Q = 0.101 m³/s, Fr_1 = 1.2, z/d_1 = 0.1; Tangential stresses and difference between the third and first quartiles of the tangential stresses were offset by +0.1m²/s²; Dimensionless time = 0 at gate closure.

6. CONCLUSION

New experiments were conducted in a large flume to investigate breaking bores and the bore roller propagation. The results demonstrated several key features of tidal bores propagating in rectangular channels. The propagation of the breaking bore roller was a highly turbulent process. Although the transverse shape of the roller toe perimeter was quasi two-dimensional on average, its shape fluctuated rapidly with transverse distance and time and the sidewalls had little effect, within the experimental flow conditions. The celerity of the roller toe fluctuated rapidly with both longitudinal and transverse distances, although almost in a two-dimensional fashion on average. Large fluctuations in breaking bore

celerity were observed. The instantaneous longitudinal free-surface profile of the roller showed significant temporal and spatial fluctuations. The free-surface fluctuations were maximum shortly after the toe passage. In comparison, undular bores presented smaller free-surface fluctuations, although these presented some periodic pattern. For $Fr_1 < 2$, a gradual rise in free-surface was observed ahead of the turbulent roller toe. The bore roller toe elevation and fluctuations in vertical elevation of toe decreased with increasing Froude number.

The unsteady velocity measurements indicated large and rapid fluctuations of all velocity components during the bore passage. The bore front passage was associated to a rapid deceleration followed by large velocity fluctuations, comparatively larger in breaking than undular bores. The velocity fluctuations yielded very significant Reynolds stress amplitudes and fluctuations. Instantaneous stress magnitudes in excess of 90 Pa were observed in laboratory, having the potential to scour large non-cohesive materials.

This study showed that the propagation of breaking bore was a complicated unsteady turbulent process. The rapid fluctuations in roller toe perimeter and free-surface profiles, as well as in all three velocity component, indicated a strongly three-dimensional turbulent flow motion.

ACKNOWLEDGMENTS

The authors thank Professor Pierre Lubin (University of Bordeaux, France) for his personal involvement, contribution and comments to the research project. They acknowledge the technical assistance of Jason Van Der Gevel and Stewart Matthews (The University of Queensland). The financial support through the Australian Research Council (Grant DP120100481) is acknowledged.

REFERENCES

Bernal, L.P., Roshko, A. (1986). Streamwise vortex structure in plane mixing layers, *J. Fluid Mech.*, 17:499–525.

Brocchini, M., Peregrine, D.H. (2001) The dynamics of strong turbulence at free surfaces. Part 2. Free-surface boundary conditions, *J. Fluid Mech.*, 449:255–290.

Bryson, A.E. (1969). Film Notes for Waves in Fluids, *Natl. Committee Fluid Mech.*, Films 21611, 8 pages.

Chachereau, Y., Chanson, H. (2011), Free-surface fluctuations and turbulence in hydraulic jumps, *Exp. Thermal Fluid Sci.*, 35(6):896–909, http://dx.doi.org/10.1016/j.expthermflusci.2011.01.009.

Chanson, H. (2010). Unsteady Turbulence in Tidal Bores: Effects of Bed Roughness. *Journal of Waterway, Port, Coastal, and Ocean Engineering ASCE*, 136(5):247-256 (DOI: 10.1061/(ASCE)WW.1943-5460.0000048).

Chanson, H. (2011) *Tidal Bores, Aegir, Eagre, Mascaret, Pororoca: Theory and Observations*, World Scientific, Singapore, 220 pages.

Chanson, H. (2012). Momentum considerations in hydraulic jumps and bores, *J. Irrigation Drainage Eng. ASCE*, 138 (4) (2012) 382–385, http://dx.doi.org/10.1061/(ASCE)IR.1943-4774.0000409.

Chanson, H., Toi, Y.H. (2015). Physical Modelling of Breaking Tidal Bores: Comparison with Prototype Data. *Journal of Hydraulic Research IAHR*, Vol. 53 (DOI: 10.1080/00221686.2014.989458)

Docherty, N.J., CHANSON, H. (2012). Physical Modelling of Unsteady Turbulence in Breaking Tidal Bores. *Jl of Hydraulic Engineering ASCE*, 138(5):412-419 (DOI: 10.1061/(ASCE)HY.1943-7900.0000542)

Goring, D.G., Nikora, V.I. (2002). Despiking Acoustic Doppler Velocimeter Data. *Jl of Hyd. Engrg*. ASCE, 128(1):117-126.

Henderson, F.M. (1966). *Open Channel Flow*, MacMillan Company, New York, USA.

Hornung, H.G., Willert, C., Turner, S. (1995). The flow field downstream of a hydraulic jump, *J. Fluid Mech.* 287, 299–316.

Koch, C., Chanson, H. (2009). Turbulence measurements in positive surges and bores, *J. Hydraulic Res. IAHR,* 47(1) 29–40, http://dx.doi.org/10.3826/jhr.2009.2954.

Kucukali, S., Chanson, H. (2008). Turbulence measurements in hydraulic jumps with partially-developed inflow conditions, *Exp. Thermal Fluid Sci.*, 33(1):41–53, http://dx.doi.org/10.1016/j.expthermflusci.2008.06.012

Leng, X. and Chanson, H. (2014) Turbulent advances of breaking bores: experimental observations. *Hydraulic Model Report CH96/14*, School of Civil Engineering, The University of Queensland, Brisbane, Australia, 42 pages.

Liggett, J.A. (1994). *Fluid Mechanics*, McGraw-Hill, New York, USA.

Lighthill, J. (1978). *Waves in Fluids*, Cambridge University Press, Cambridge, UK, 504 pages.

Madsen, P.A. (1981). A model for a turbulent bore, *Ph.D. thesis*, Tech. Univ. of Denmark, Inst. of Hydrodynamics and Hyd. Eng., Copenhagen, Denmark, 1981, 149 pages. (also Series Paper No. 28, Tech. Univ. of Denmark, Inst. of Hydrodyamics and Hyd. Eng., Copenhager, Denmark, 149 pages.).

Misra, S.K.,Thomas, M., Kambhamettu, C, Kirby, J.T., Veron, F., Brocchini, M. (2006) Estimation of complex air–water interfaces from particle image velocimetry images, *Exp. Fluids*, 40:764–775, http://dx.doi.org/10.1007/s00348-006-0113-1.

Mouaze, D., Murzyn, F., Chaplin, J.R. (2005) Free surface length scale estimation in hydraulic jumps, *J. Fluids Eng. ASME*, 127:1191–1193.

Murzyn, F., Mouaze, D., Chaplin, J.R. (2007). Air–water interface dynamic and free surface features in hydraulic jumps, *J. Hydraulic Res. IAHR*, 45(5):679–685.

Murzyn, F., Chanson, H. (2009). Free-surface fluctuations in hydraulic jumps: experimental observations, *Exp. Thermal Fluid Sci.*, 33(7):1055–1064.

Rayleigh, Lord (1908). Note on tidal bores, *Proc. Royal Soc. London, Ser A*, Contain. Papers Math. Phys. Charact. 81 (541) 448–449.

Richard, G. (2013). Élaboration d'un modèle d'écoulements turbulents en faible profondeur: Application au ressaut hydraulique et aux trains de rouleaux, ('Elaboration of a model of turbulent shallow water flows: Application to the hydraulic jump and roll waves.') *Ph.D. thesis*, University of Aix-Marseille, Institut Universitaire des Systèmes Thermiques Industriels IUSTI, France, 212 pages (in French).

Shields, A. (1936) *Anwendung der Ähnlichkeitsmechanik auf die Geschiebebewegung*. (Mitt. der Preussische Versuchanstalt für Wasserbau und Schiffbau: Berlin, Germany), No. 26.
Spiegel, M.R. (1972) *Theory and Problems of Statistics*, McGraw-Hill Inc., New York, USA.
Tricker, R.A.R. (1965). *Bores, Breakers, Waves and Wakes*, American Elsevier Publ. Co., New York, USA.
Valiani, A. (1997). Linear and Angular Momentum Conservation in Hydraulic Jump. *J Hydraulic Res. IAHR*. 35(3) 323-354
Wahl, T.L. (2003). Despiking Acoustic Doppler Velocimeter Data. Discussion. *Jl of Hyd. Engrg. ASCE*, 129(6):484-487.
Wang, H., Chanson, H. (2013). Free-surface deformation and two-phase flow measurements in hydraulic jumps, *Hydraulic Model Report No. CH91/13*, School of Civil Engineering, The University of Queensland, Brisbane, Australia, 108 pages (ISBN 9781742720746).
Wang, H., Murzyn, F., Chanson, H. (2014). Total pressure fluctuations and two-phase flow turbulence in hydraulic jumps, *Exp. Fluids*, 55(11), Paper 1847, 16 pages, http://dx.doi.org/10.1007/s00348-014-1847-9.
Yalin, M. S., and Karahan, E. (1979) Inception of sediment transport. *Journal of Hyd. Div.*, 105, No. HY11, 1433-1443
Yeh, H.H., Mok, K.M. (1990) On turbulence in bores, *Phys. Fluids A*, A2(5):821-828.